universe

MDPI

Article

Analysis of the Ionospheric Response to Sudden Stratospheric Warming and Geomagnetic Forcing over Europe during February and March 2023

Rumiana Bojilova * **and Plamen Mukhtarov**

National Institute of Geophysics, Geodesy and Geography-Bulgarian Academy of Sciences, Acad. G. Bonchev Str., bl. 3, 1113 Sofia, Bulgaria; engpjm@abv.bg
* Correspondence: rbojilova@geophys.bas.bg; Tel.: +359-029-793-308

Abstract: A study of the behavior of the main characteristics of the ionosphere over Europe during the 26–28 February 2023 ionospheric storm was carried out in this present work. The additional influence of sudden stratospheric warming on the ionosphere was considered. The behavior of the critical frequency of the ionosphere foF2 (characterizing the maximum electron density), the peak height of the F2-layer (hmF2), and Total Electron Content (TEC) were investigated through their relative deviations from the quiet conditions. The behavior of the TEC over Europe showed the geographic latitudinal dependence of the response. The variability in the ionospheric critical frequency was represented by the data of 10 ionospheric stations for vertical sounding located in two groups: (i) near the prime meridian and (ii) near the 25° E meridian. Some differences were found in the response compared to the TEC response, which was explained by the different responses of the top maximum region and bottom maximum region. The peak height of the F2 layer varied strongly during the storm, which was due to the forced drift of ionospheric plasma induced by additional electric fields. The present detailed analysis of the ionospheric response shows that the considered storm exhibited characteristic features inherent in the winter season but with some manifestations of reactions in equinox conditions.

Keywords: ionospheric storm; critical frequency; TEC; hmF2; geomagnetic storm

check for updates

Citation: Bojilova, R.; Mukhtarov, P. Analysis of the Ionospheric Response to Sudden Stratospheric Warming and Geomagnetic Forcing over Europe during February and March 2023. *Universe* **2023**, *9*, 351. https://doi.org/10.3390/universe9080351

Academic Editors: Mingxian Zhao and Jianyong Lu

Received: 29 June 2023
Revised: 25 July 2023
Accepted: 26 July 2023
Published: 28 July 2023

1. Introduction

The changes in electron density and the response of the ionosphere during geomagnetic storms have been sufficiently studied and described during the last few decades. The processes in the ionosphere during a geomagnetic storm triggered by particle precipitation into auroral ovals have been studied in sufficient detail [1–5]. In these papers, the main mechanisms of the ionospheric response to geomagnetic storms have been largely clarified by the change in the atomic oxygen–molecular nitrogen (O/N_2) ratio under the action of the thermal effect of Joule heating and the disturbance of atmospheric dynamics associated with the Equatorial Ionospheric Anomaly (EIA). The O/N_2 composition of the thermosphere is the main factor describing changes in electron density [6].

The main mechanisms of impact of geomagnetic storms on the ionospheric electron concentration in mid-latitudes are decreases in O/N_2 due to Joule heating in the auroral oval and the transport of neutral air with a changed O/N_2 ratio in mid-latitudes from the meridional circulation, the seasonal features of which determine seasonal differences in ionospheric response. In addition to this mechanism, the mechanism of changing the dynamics in tropical latitudes also operates, the changes of which (the so-called "disturbed dynamo") affect the vertical drift of the ionospheric plasma and, accordingly, the "fountain effect", and the variations in the electron concentration caused by it can also spread to mid-latitudes. In recent years, following the launch of satellites such as GOLD, SWARM, and GUVI, investigations have been carried out that have significantly contributed to the understanding of the effects that O/N_2 change has on the ionosphere [7–9].

Another phenomenon, the so-called EIA, is due to the reduction in plasma in the equatorial region, which moves and accumulates at ~±20° magnetic latitudes. The intense EIA under magnetically active conditions is due to the combined impulsive action of eastward prompt penetration electric fields and equatorward neutral wind [10].

Again, it is good to note the introduction of modernized measurements in the study of the ionospheric response and, in particular, the behavior of the EIA under conditions of geomagnetic storms. Using data from the Global-scale Observations of the Limb and Disk (GOLD) mission has allowed the effects of geomagnetic disturbances on ionospheric variations to be examined. A recent study of the impact of the 23–29 September 2020 storm on the behavior of the equatorial ionosphere at night showed the following results: favorable conditions for the penetration of interplanetary electric fields to the equatorial ionosphere (~35° W Lon) were observed on September 27. The additional enhancement of the fountain effect was found as a consequence of an increase in prompt penetration electric fields (PPEFs). An increase in the height of the F2 ionospheric layer was also obtained in this study [11]. A very recent investigation of the EIA response to the geomagnetic storm of 3–4 November 2021 showed a structure of a merged EIA with one density crest located near the magnetic equator on 4 November 2021. Using a first-principles model, the authors analyzed the merged EIA structure. The results showed that the geomagnetic disturbance considered by the authors caused disturbances in thermospheric neutral winds [12].

Another interesting phenomenon related to the response of the ionosphere in the northern hemisphere is due to the additional ionization caused by the particle precipitation of solar wind. In one study regarding the response to the ionosphere during the geomagnetic storm on 25–26 August 2018, the authors established that the TEC enhancement at high latitudes should have been due to particle precipitation [13]. An investigation studied the influence of direct ionization in the auroral oval on the TEC in winter conditions, the results of which showed that the zone of the direct influence of particle precipitation is between inclinations of 70° and 80° [14]. In this article, it is emphasized that when using the relative deflection of the TEC, the effect is particularly noticeable in cases where the TEC has small values (during winter-time or in night-time conditions).

One significantly important ionospheric phenomenon has been the subject of a number of studies in recent years, namely Sudden Stratospheric Warming (SSW). This phenomenon is a meteorological event that can last several days or even weeks in the winter hemisphere [15]. Changes in the stratosphere under SSW conditions are associated with a sharp rise in temperature, a change in the direction and shape of the normal winter polar vortex, and a decrease and even a change in the direction of zonal winds [16]. The influence of SSW on the ionosphere–thermosphere system was studied, and it was found that during the positive phase, the equatorial ionization anomaly is enhanced as the ridges move to higher latitudes, while during the negative phase, the equatorial ionization anomaly is suppressed [15]. The semidiurnal behavior of warming in the lower thermosphere and cooling in the upper thermosphere is the effect that causes SSW at mid-latitudes [17]. Studies of the impact of SSW on the electron density of the ionosphere date relatively recently [18–20]. These studies show that the influence of SSW on the ionospheric electron density occurs through the so-called “disturbed dynamo”, a change in the wind system in the lower thermosphere and, as a consequence, anomalies in the electric fields that shape the EIA. In one paper [21], through a statistical analysis of the period 2005–2010 using TEC data under winter conditions, it was found that variations in stratospheric temperature at 60° N latitude affect the TEC regardless of whether SSW occurs. In [22], a situation was simulated in which the October 2003 Halloween storm coincided in time with a major SSW. The author’s conclusion was that, in this case, the vertical E x B drift in the equatorial region would have differed from that in the absence of SSW.

This present study investigates the ionospheric response represented by some of the main ionospheric parameters during the 26–27 February 2023 geomagnetic storm. The behavior of the Total Electron Content (TEC), critical frequency of the ionospheric F region (foF2), and the peak height of the F2-layer (hmF2) were investigated. The research is concentrated on the European ionosphere, but some aspects of the global response are also affected. An interesting feature of the considered geomagnetic storm is that it takes place in the conditions of major SSW, in which the influence of processes in the middle atmosphere on the ionosphere is combined with the influence of the solar wind. For this reason, the event is a complex manifestation of the so-called forcing from below and forcing from above. In this present work, an attempt is made to investigate the joint influence of a geomagnetic storm and SSW in real conditions.

2. Data and Methods

The present investigation used the following types of parameters, as outlined in this section.

2.1. Parameters, Describing the Geomagnetic Storm

Solar indices are the Bz component of the interplanetary magnetic field (IMF) and density of solar wind. All these solar wind components are according to the NASA Advanced Composition Explorer (ACE) satellite (ftp://ftp.swpc.noaa.gov/pub/lists/ace/, accessed on 2 March 2023). The geomagnetic activity is described by the Dst index and planetary Kp index; both types of data were received from Goddard Space Flight Center (https://omniweb.gsfc.nasa.gov/, accessed on 20 March 2023). The data of solar activity, described by the solar radio flux at 10.7 cm, were taken from https://omniweb.gsfc.nasa.gov/, accessed on 10 March 2023. The Power index, which is an estimate of the energy entering the Earth's polar regions, was obtained from NOAA, Space Weather Prediction Center (http://services.swpc.noaa.gov/text/aurora-nowcast-hemi-power.txt, accessed on 2 March 2023). Power index values for both hemispheres are summed. Stratospheric temperature and wind speed data were obtained from the NOAA Climate Prediction Center (https://www.cpc.ncep.noaa.gov/products/monitoring_and_data/oadata.shtml, accessed on 20 March 2023).

2.2. Ionospheric Parameters from GIRO

Data from the vertical sounding of the ionosphere are taken from the Global Ionosphere Radio Observatory (GIRO) (https://giro.uml.edu/index.html, accessed on 25 July 2023). The following ionospheric parameters from the GIRO database will be used in this present work: the critical frequency of the F2 region (foF2) and the peak height of F2-layer (hmF2). The ionospheric stations, data from which are used in this present work, are grouped into two groups: Western European and Eastern European. The Western European group, including stations EA036, DB049, and FF051, is located between geomagnetic latitudes from 41.4° N to 54.3° N and between geomagnetic longitudes from 72.3° W to 88.51° W (see Table 1). Accordingly, the Eastern European group is between geomagnetic latitudes from 31.7° N to 54.19° N and between geomagnetic longitudes from 98.23° E to 111.0° E. The second Eastern European group includes the NI135, AT138, VT139, SO148, PQ052, MZ152, and JR055 ionospheric stations. The data from the ionospheric stations, which are every 15 min, are averaged to 1 h. Values that differed from the monthly mean at a given hour by more than three times the standard deviation calculated over all data for the month were removed [23]. In this present work, the relative deviations of the ionospheric quantities foF2, hmF2, and TEC from the quiet conditions represented by the monthly medians are used [14].

Table 1. The groups of ionospheric stations used are Western European (upper part of stations) and Eastern European (lower part of stations).

STATION CODE	STATION NAME	LAT	LONG	MLAT	MLON
EA036	EL ARENOSILLO	37.1	−6.7	41.4	72.3
DB049	DOURBES	50.1	4.6	51.26	88.51
FF051	FAIRFORD	51.7	−1.8	54.3	82.8
NI135	NICOSIA	35.0	33.2	31.7	111.0
AT138	ATHENS	38.0	23.6	36.4	102.5
VT139	SAN VITO	40.6	17.8	39.89	98.29
SO148	SOPRON	47.7	16.1	45.9	101.3
PQ052	PRUHONICE	50.0	14.6	49.55	98.23
JR055	JULIUSRUH	54.6	13.4	54.19	99.03

2.3. TEC Data

In this study, we used vertical TEC maps generated by the Center for Orbit Determination in Europe (CODE), which are accessible online (ftp://ftp.unibe.ch/aiub/CODE/, accessed on 25 July 2023). The time resolution of TEC data is 1 h, and the data have a grid spacing of 5° (in longitude) × 2.5° (in latitude). This type of GNSS data is widely used by scientists to study the spatial distribution of the ionospheric response during geomagnetic disturbances [14,24,25]. To examine the spatial distribution of the TEC response, the relative deviation (*r*TEC is the same as relative TEC) of its values from the hourly medians (TEC*med*) calculated over a time period of 27 days centered on the current day is used.

$$rTEC(t) = \sqrt[3]{\frac{TEC(t)}{TEC_{med}(UT)}} - 1 \quad (1)$$

The proposed formula for relative deviation of TEC (abbreviation "Relative TEC" will be used in the text) is applied in cases in which the median values become small, even zero. In many cases, in night-time conditions at high latitudes during the winter season, the average values become small, sometimes even zero. During geomagnetic storms, as a result of the additional ionization from the particle precipitation, a sharp increase in TEC is observed, which is observed in the median values. The use of Formula (1) allows reliable results to be obtained for high latitudes during the winter season in geomagnetic storm conditions, such as the case considered in this investigation. One physical explanation for the use of Formula (1) is related to the presence of additional ionization from particle precipitation in the polar regions under night-time conditions, resulting in additional electron density being added to the existing one. The use of relative deviation in the ionospheric parameters allows us to give an estimate of the response of the ionosphere to quiet conditions [14].

The relative deviations of the critical frequencies and the peak height of F2-layer are calculated using the traditional method as follows:

$$rfoF2(t) = \frac{foF2(t) - foF2_{med}(UTC)}{foF2_{med}(UTC)} \quad (2)$$

$$rhmF2(t) = \frac{hmF2(t) - hmF2_{med}(UTC)}{hmF2_{med}(UTC)} \quad (3)$$

where *foF2*(*t*) and *hmF2(t)* correspond to the measured value of the critical frequency of the ionospheric F2 layer and the peak height of F2-layer, while *foF2med(UTC)* and *hmF2 (UTC)* are the median values of the same quantity.

With these two ionospheric features, the problem that exists with the TEC data from CODE does not exist. The minimum values of foF2 cannot be smaller than 1.5 MHz, which is related to the capabilities of the ionosondes for vertical sounding.

3. Results

In this section, the possible causes of the electron density changes in February 2023 will be considered, namely (i) SSW, (ii) changes in solar and geomagnetic activity, and (iii) the parameters characterizing the geomagnetic storm. Comparative maps for the spatial distribution of the ionospheric response are presented for the considered ionospheric parameters hmF2, foF2, and TEC.

3.1. Stratospheric Warming and Solar and Geomagnetic Influences on Ionospheric TEC in February and March 2023

The impact of Sudden Stratospheric Warming on the thermosphere–ionosphere system is well known and studied in detail [26–30]. That is why special attention will be paid to this phenomenon and its manifestation. Stratospheric warming during February and March begins on 15 February 2023 with a temperature rise at the 10 hPa (32.5 km) level (top panel) and a reversal of the zonal wind direction (middle panel). On 5 March, the area with negative wind values (east–west direction) reaches a height of 20 km. Recovery of the positive wind direction at 10 hPa occurs on 11 March (see Figure 1, middle panel). By definition, this stratospheric warming is major [31].

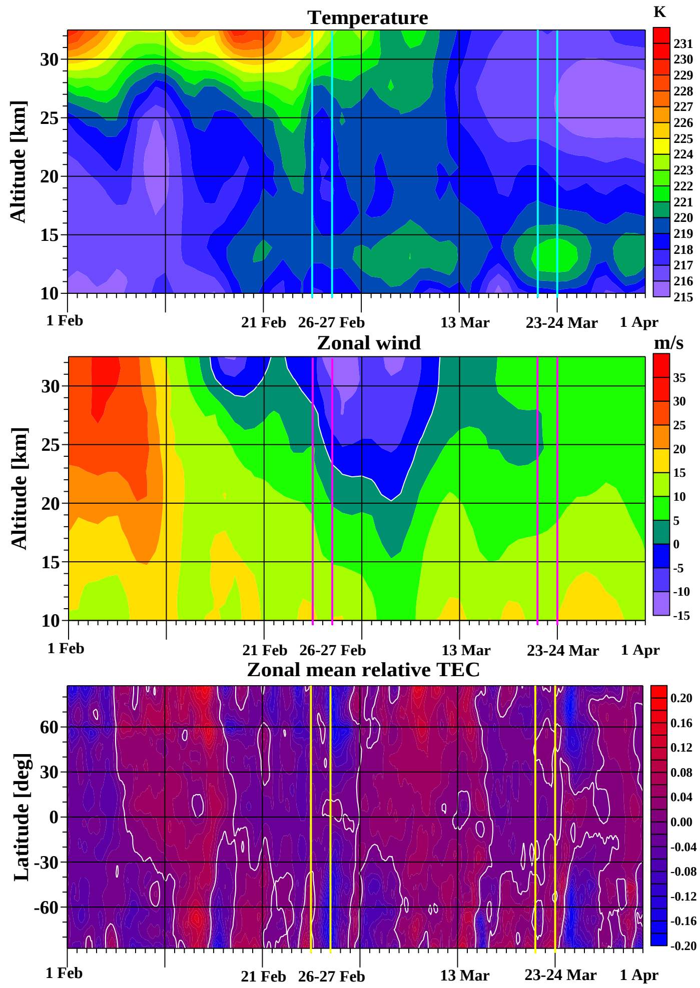

Figure 1. Trends of zonally averaged stratospheric temperature (**top** panel), zonal wind (**middle** panel), and zonal mean relative TEC (**bottom** panel) during the months of February and March 2023.

As a feature of the general state of the ionospheric TEC, Figure 1 (bottom panel) shows a map of the latitudinal distribution of the zonal mean relative TEC smoothed with 25 hourly moving averages. The ionospheric TEC response to the 26–27 February 2023 geomagnetic storm will be discussed in detail below. At this stage, it is sufficient to note that after the begging of the storm at the equator, the zonal mean values of the relative TEC increase, while, at other latitudes, the reaction is clearly negative. A similar reaction was observed during the geomagnetic storm on 23–24 March 2023, which occurred in a period of almost zero values of the relative TEC. The geomagnetic storm investigated in this present work entirely takes place under conditions of stratospheric warming (see Figure 1), which has an additional impact on the ionosphere.

In order to evaluate the influence of the other factors that affect the TEC, individually from the geomagnetic disturbance, Figure 2 shows the course of the geomagnetic indices Dst, Kp, and the radio emission flux F10.7 during February and March 2023. The first quantity characterizing the equatorial ring current, namely Dst for these two months clearly shows three disturbances in the days: 15–16 February, 27 February, and 24 March 2023 (see Figure 2, top panel). According to the classification, the first event is of the Moderate class, and the second and third are of type Strong (i.e., intense) [32]. During the same period, three increases in solar activity represented by F10.7 were also recorded, with maxima around 11 February, around 6 March, and around 25 March (see Figure 2, middle panel). During the considered period, three geomagnetic storms were registered according to the planetary Kp index: (1) 15–16 February, with Kp values around 5; (2) on 26–27 February, Kp is about 5.33; on 23–24 March, Kp reaches 8 (for reference see Figure 2, bottom panel).

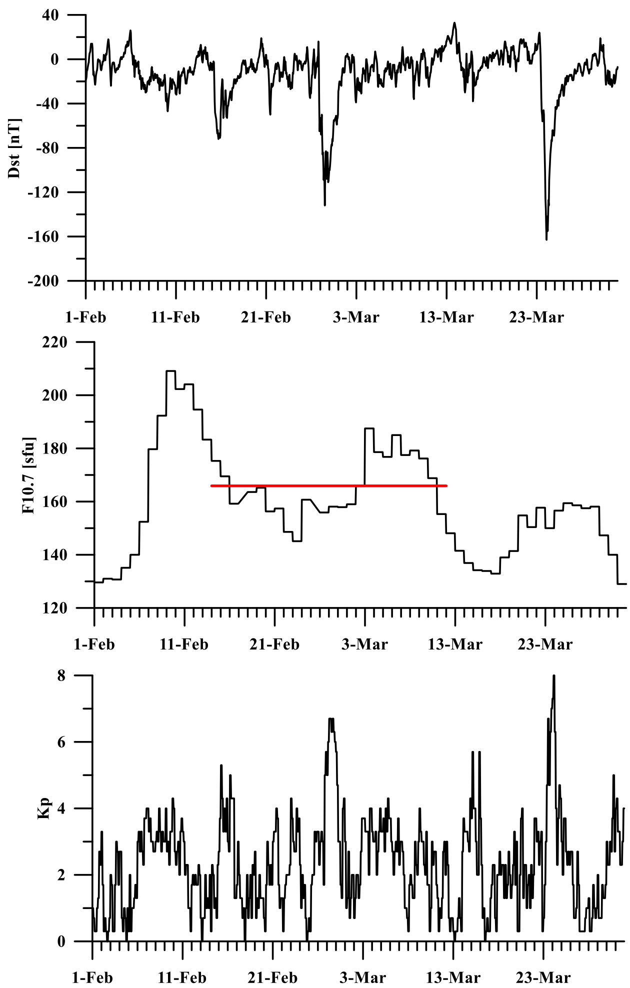

Figure 2. Variations of solar activity represented by F10.7 (**middle** panel) and geomagnetic activity represented by Dst (**top** panel) and Kp (**bottom** panel) during the months of February and March 2023.

In Figure 2, the red line shows the average value of F10.7 over a period of 27 days centered on the date of 26 February when the geomagnetic storm, which is the subject of investigation in this work, started. Considering that the relative TEC is calculated to segment 27-day moving medians, on the day before the storm, the solar activity level is close to the average for the period for which the moving medians are calculated, and it would be expected that rTEC should have values close to zero. Such a situation is observed at high mid-latitudes, but at low latitudes and at the equator, the relative deviation before the storm is negative, around 0.05, indicating that the storm starts in conditions where TEC is influenced by stratospheric warming with a negative response to zonal mean values at low latitudes.

Figure 3 shows the relative TEC values for the equator, 30° S, 30° N, 60° S, and 60° N, which allows for the consideration of the influence of variations in solar and geomagnetic activity when diurnal and longitudinal variations are eliminated. The increase in relative TEC until 11 February is most likely due to the increase in solar activity. The weak geomagnetic storm on 15 February causes a negative ionospheric response at the mid-latitudes and a positive one in the equatorial region. Stratospheric warming also begins on the same date. According to the study of the response of zonal mean TEC to stratospheric warming, a negative response is observed that increases towards tropical latitudes [18,21]. In this particular case, relative TEC decreases and becomes negative at low latitudes under both stratospheric warming and the decrease in F10.7 after 11 February. It can be seen in Figure 3 that a change in the relative deviation of TEC of 0.1 means an increase or decrease in the magnitude by about 30% (i.e., 0.3 according to the cubic root in Formula (1)).

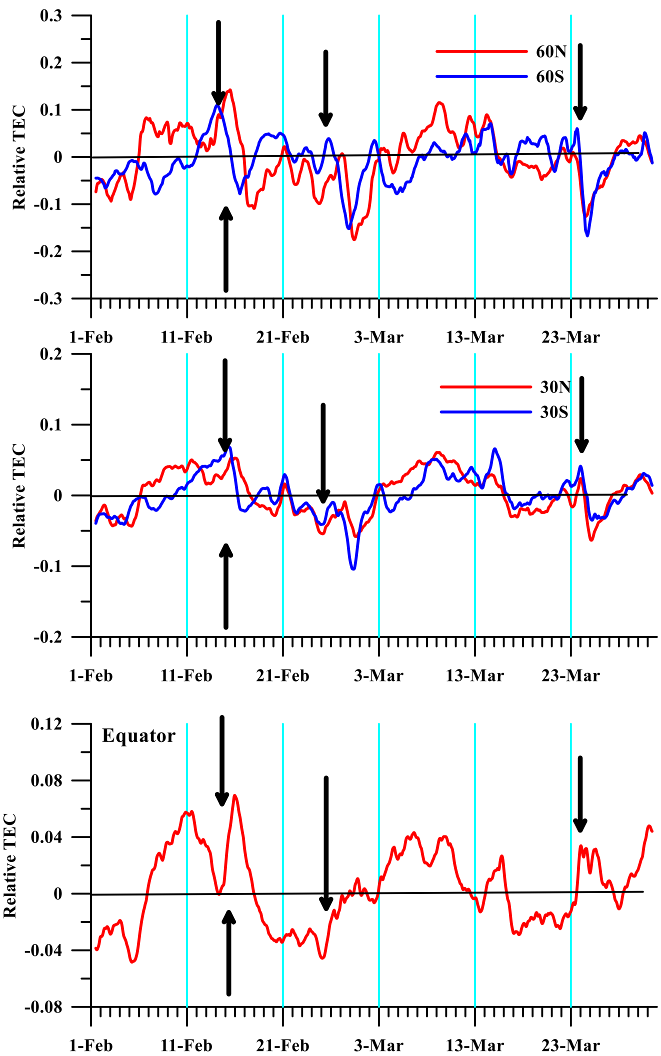

Figure 3. Variations of the zonal mean value of the relative TEC for latitudes 0° (**bottom** plot), ±30° (**middle** plot), and ±60° (**top** plot) during the months of February and March 2023. Values for the Northern Hemisphere are marked in blue, and values for the Southern Hemisphere are marked in red.

3.2. Ionospheric Response during Geomagnetic Storm

3.2.1. Variations of Geomagnetic and Solar Parameters during the Geomagnetic Storm on 26–27 February 2023

The manifestation and influence of geomagnetic storms on the electron density and behavior of the ionosphere is an actual and interesting task on which scientists have been working hard in recent decades [4,5,33–37]. Some parameters are well known, which help in the analysis of ionospheric disturbances. Used in this present study to track the behavior of the geomagnetic disturbance on 26–27 February are as follows: (a) Dst index, which gives information about the strength of the ring current around Earth caused by solar energetic particles; (b) Kp index is a three hourly index, which is used to characterize the magnitude of geomagnetic storms; (c) Power index describing the flux of energy entering the Earth's polar regions; (d) the last three components are widely used to estimate the impact between the charged particles of the Sun and the Earth, namely Bz (the vertical component of the interplanetary magnetic field), Density of solar wind, and the Speed.

According to Figure 4 (right panel, top plot), the sharp transition of the vertical component of the interplanetary magnetic field Bz (data are discrete at 1 min intervals) occurs at 18:50 UT on 26 February. The distance between the satellite and the Earth is 1.5 million km. At a solar wind speed of about 500 km/s, this distance is traveled in about 50 min [38]. It follows that the beginning of the storm can be assumed to be 19:30 UT, which coincides with the increase in the Power index, the data for which are discrete with an interval of 5 min. At 20 UT on 26 February, the Kp index becomes 5, and Dst becomes around −40 nT. Kp is above 5 between 20 UT on 26 February and 2 UT on 28 February. The maximum of the storm can be considered to be around noon time on 27 February. Around 12 UT, the Kp index exceeds 6, while Dst is between −130 and –140 nT, which corresponds to Strong (i.e., intense) disturbance. At the same time, the Power index has a maximum value of about 300 GW. Then, the recovery phase begins.

3.2.2. Ionospheric Variations in the Initial Phase of the Storm

The relative TEC maps (top panels) for the Northern Hemisphere at longitudes 00° E and 25° E shown in Figure 5 illustrate the main responses of the ionospheric electron density in the European region for the period of 26–28 February 2023. At 60° N, the positive response of this latitude characteristic of the winter season is observed at a local time close to midnight, which is due to ionization by charged particles of the solar wind entering the auroral oval [14]. The constructed map of relative foF2 drift in Figure 5 (bottom panel) shows considerable similarity to the 25° E TEC map for latitudes between 35° N and 55° N. A significant difference is observed between 16 UT and 18 UT on 26 February. In this period, all ionospheric stations show a positive response, which is missing and absent in TEC.

Figure 6 presents the beginning of the storm with a dashed line. Before it, the relative critical frequencies obviously increase, and after it, a decrease begins, which is observed in all ionospheric stations. The phenomenon, however, is absent in TEC (see Figure 5, top row of panels). It can be hypothesized that this phenomenon is caused by intra-atmospheric causes associated with stratospheric warming, which on 26 February 2023 is close to its maximum. A possible reason for the absence of a positive reaction in TEC is compensation for the increase in the electron density around the maximum with its decrease in the region above the maximum.

The peak height response of the ionospheric electron density maximum, represented by the relative deviation, is shown in Figure 7. It shows the different behaviors in Western Europe and Eastern Europe. Figure 7 illustrates that the two West European stations (top panel) show a small positive response until 20 UT (DB049 and FF051). Another station EA036 and all stations in the East European sector recorded a decrease in hmF2 before the onset of the storm. A sharp decrease is observed in all stations at 20 UT, and the strongest negative response is in the southern stations (NI135 and AT138). Figure 7 shows that the negative ionospheric response is stronger in the Eastern Europe chain than in the Western Europe chain. The relative deviation response of hmF2 clearly shows a latitudinal dependence. The most significant negative response up to about −0.15 is observed in ionospheric stations NI135 and AT138, part of the Eastern Europe sector (see Figure 7, bottom panel). Following the response to the north, stations SO148 (Eastern Europe chain) and FF051 (Western Europe chain) also react negatively at about 20 UT, although the hmF2 values do not cross 0. The response in these stations is much weaker than in the others. A possible explanation for the more significant response in low latitudes is related to EIA effects.

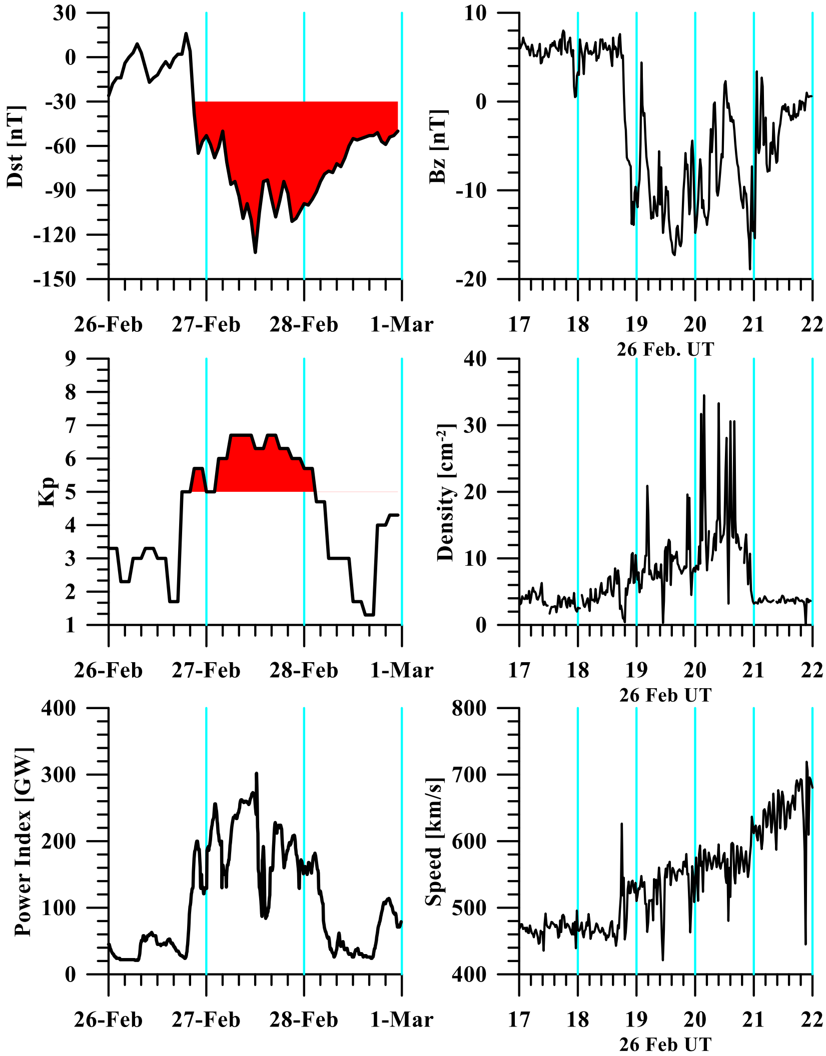

Figure 4. Behavior of geomagnetic indices Dst (**left** panel, **upper** plot), Kp (**left** panel, **middle** plot), and Power index (**left** panel, **bottom** plot). The figure also presents the parameters of solar wind: Bz (**right** panel, **top** plot), Density (**right** panel, **middle** plot), and Speed (**right** panel, **bottom** plot).

The analogous reaction can be seen in spatial distribution for the Eastern Europe sector illustrated in Figure 8. The idea of this figure is to follow in more detail the distribution of the response of the hmF2 relative deviation in the period of 26–28 February 2023. For this purpose, the data from the six stations of Eastern Europe were taken, and via interpolation, the shown map was obtained. Figure 8 shows the regions of negative response between 16 UT and 20 UT at latitudes between 35.0° and 41.5° and also between 47.5° and 52.0°, where almost all of the considered ionospheric stations are located. After 20 UT at all latitudes, the hmF2 response becomes positive, which is an analogous result to Figure 7, bottom panel.

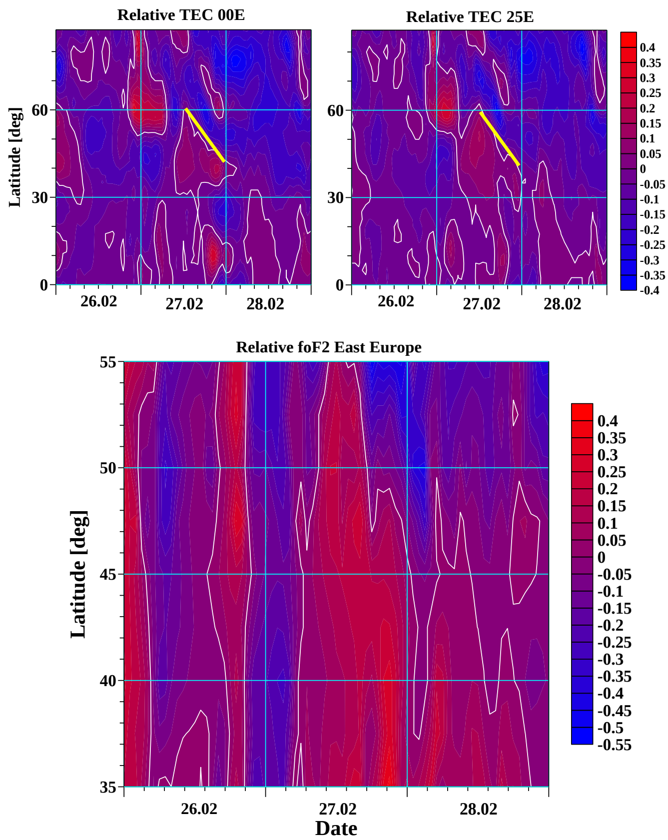

Figure 5. Variations of the relative TEC and relative foF2 over Europe.

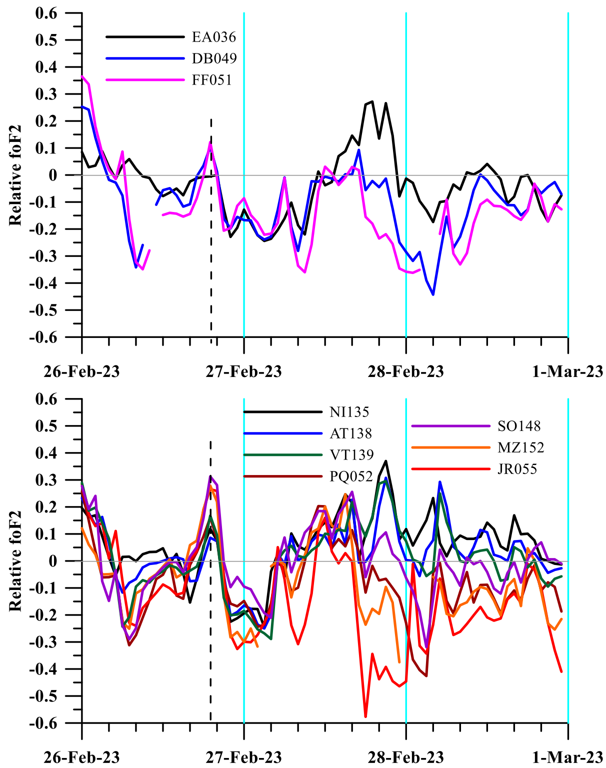

Figure 6. Behavior of relative critical frequencies of stations in Western Europe (**upper** panel) and Eastern Europe (**bottom** panel). The onset of the geomagnetic storm is marked with a dashed line in the figure.

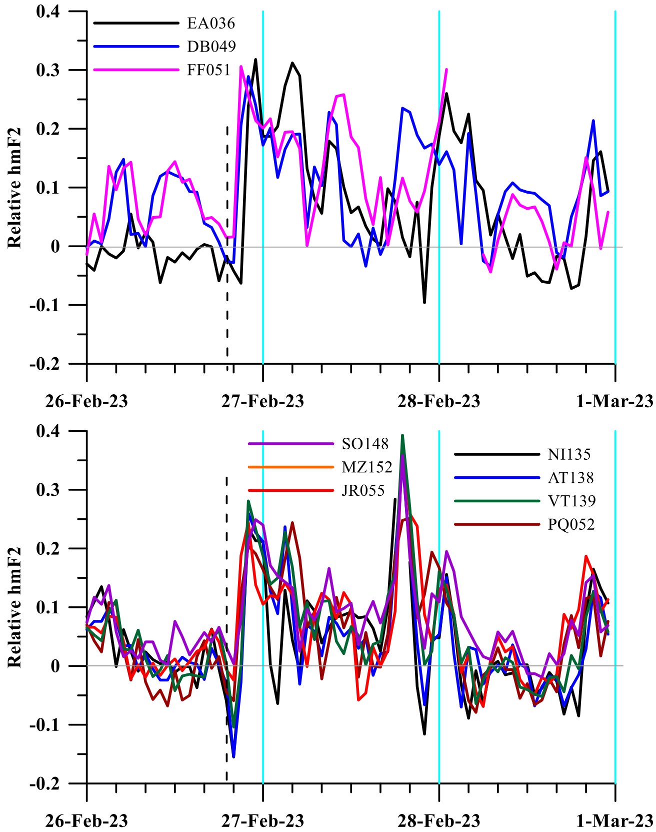

Figure 7. Behavior of relative values of peak height of the F2-layer of stations in Western Europe (**upper** panel) and Eastern Europe (**bottom** panel). The onset of the geomagnetic storm is marked with a dashed line in the figure.

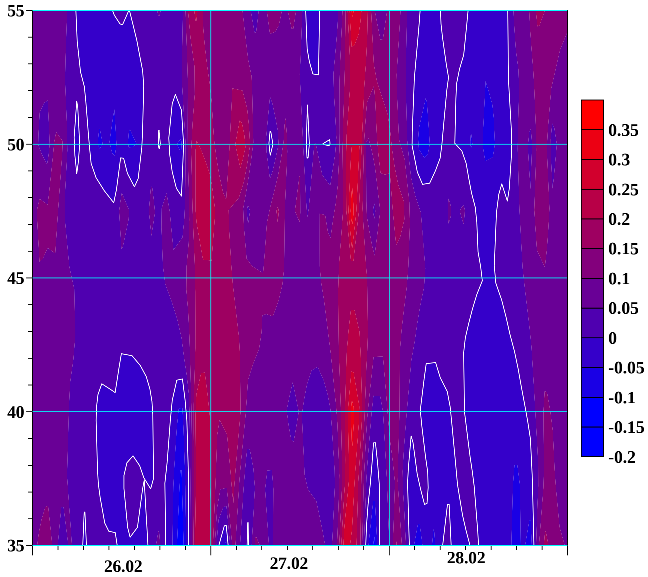

Figure 8. Spatial distribution of variations in the relative peak height of the ionospheric maximum for Eastern Europe sector.

Figure 9 shows the variability of the values of the relative critical frequencies and the relative values of hmF2 with a step 15 min before the onset of the storm and in its initial phase (from 12 UT to midnight on 27 February). It is noticed that from 17 UT, a simultaneous increase in the critical frequencies and a decrease in the peak height of the

F2-layer, which should not be the result of the geomagnetic disturbance. After the onset of the geomagnetic storm, the decrease in hmF2 occurs until about 21 UT, when a sharp increase in hmF2 begins. A similar effect was observed during the winter geomagnetic storms in January 2005 [39]. The considered variations of the ionospheric characteristics before and immediately after the onset of the storm suggest that during this time period, the ionosphere is influenced by two processes: one of them with an intra-atmospheric origin and the other with an influence of geomagnetic activity.

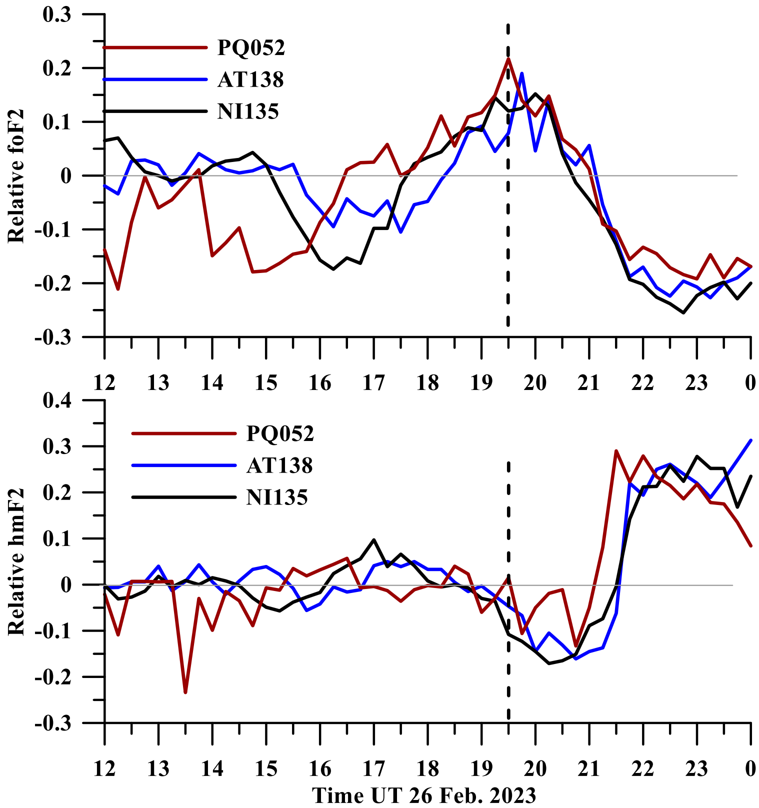

Figure 9. Variations of relative critical frequencies and peak height of F2-layer of the maximum before and at storm onset. The onset of the geomagnetic storm is marked with a dashed line in the figure.

The observed positive anomaly in the critical frequencies of many of the ionospheric stations before the onset of the geomagnetic storm can also be considered a manifestation of the phenomenon of prestorm deviations (or ionospheric precursors), which is the subject of extensive discussion in scientific investigations. The results of the research on this issue are analyzed and summarized in detail [40,41]. Based on statistical studies, some authors conclude that the observed anomalies in the ionospheric electron density before the onset of the geomagnetic storm are related to it [42]. Some authors note that there are no proven physical mechanisms to explain these anomalies occurring before the onset of the geomagnetic storm [43]. Other authors conclude that the observed anomalies are due to internal atmospheric processes and are not related to geomagnetic storms. In the present investigation, it is considered the hypothesis of the most likely cause of the observed anomaly, which is caused by its intra-atmospheric origin.

3.2.3. Ionospheric Variations during the Main Phase of the Storm

Between 20 UT on 26 February and 05 UT on 27 February, the mid-latitude TEC and foF2 response in night-time conditions is negative. A statistically summarized and detailed examination of the TEC response in winter conditions shows the appearance of a region of negative response in mid-latitudes in the hours after midnight in local time, immediately south of the region of positive response in auroral latitudes [44]. The reason for this reaction can be the transfer of warm air from the auroral oval and a corresponding change in the O/N_2 ratio, respectively, an increase in recombination, which in the absence of ionizing radiation causes a significant decrease in the electron density. There is a possible influence of the electric fields created by the anomalous dynamics of the neutral atmosphere during the storm, which also affects the ionospheric response. It is observed that the negative anomaly of TEC and foF2, according to Figure 5, Figure 6, and Figure 9 occurs almost without delay after the onset of the storm and occurs at low latitudes (stations NI135 and AT138). The peak height of the F2-layer during the night of 26 to 27 February rises after 21 UT, which is a typical reaction of the night-time mid-latitude ionosphere during a storm. Between midnight and 08 UT on 27 February, variations in relative hmF2 are observed at all stations, being strongest in southern Eastern Europe (see Figure 7, bottom panel).

The geomagnetic storm reaches its maximum around noon on 27 February, when the European region is in daytime conditions. In the hours before and around noon, the response of TEC and foF2 becomes positive, which is the result of the northward expansion of the EIA under the action of the perturbed component of the meridional wind, which in low latitudes under the influence of Coriolis acceleration deviates to a zonal direction. After 16 UT, the process of the propagation of a negative anomaly from north to south begins, which is the result of the transfer of warmed air. The decrease in electron density offsets the increase under EIA as well. The zero line in the maps in Figure 5 gives information about the speed of this penetration, which is approximately 20° (from 60° N to 40° N) in about 12 h. This means a speed of about 185 km/h (666 m/s). The resulting speed is significantly higher than the meridional wind speeds in the thermosphere [45]. Fuller-Rowell has simulated a global wind surge that has the character of a large-scale gravity wave with a phase speed of about 600 m/s [4]. The latitudinal dependence of the propagation of the negative anomaly is illustrated in great detail by the relative critical frequencies of the European ionospheric stations. The response is strongest in the northern stations (JR055 and FF051). In southern stations (NI135, AT138, VT139), the negative response is weak, and it even turns into a positive after 20 UT (see Figure 6). The possibility of excitation of a high-velocity propagating gravity wave is evident from the behavior of the peak height of the F2-layer. In Figures 7 and 8, a sharp increase in peak height of the F2-layer around 18 UT and around 02 UT on 28 February is observed. The increase is strong in the Eastern European region and weak in the Western European region.

4. Discussion and Conclusions

In this present study, an investigation of the ionospheric response is carried out in the case where exist all three factors that affect it: (i) variations in solar activity, (ii) geomagnetic storms, and (iii) Sudden Stratospheric Warming. The first two factors are of cosmic origin, while the third is of intra-atmospheric origin. The time scale of variations in the ionizing radiation of the Sun and changes in the dynamics of the neutral atmosphere caused by SSW is about one month, while the duration of a geomagnetic storm is an order of magnitude smaller. In this specific case, the known pattern of negative ionospheric electron density response during major SSW, stronger at low latitudes, is confirmed. The investigated geomagnetic storm occurs on days close to the maximum of stratospheric warming and with solar activity approximately coinciding with the average for the reference period, based on which the relative deviation of the ionospheric characteristics is calculated. For this reason, it can be argued that the predominant negative deviation from the reference state before the onset of the geomagnetic storm is due to the influence of the SSW.

The ionospheric response to the geomagnetic storm, which has been studied in detail for the European region based on TEC, foF2, and hmF2 data, clearly shows the known mechanisms of influence on the ionosphere in winter conditions [14]. The selection of the European region for the detailed study is based on the possibility of comparing the TEC data with independent data from ionospheric vertical sounding stations.

The variability of the TEC over Europe shows the geographic latitudinal dependence of the ionospheric response. Positive responses caused by the additional ionization in the auroral oval and the influence of the Equatorial Ionization Anomaly (EIA) on the mid-latitude atmosphere are observed.

The negative ionospheric responses during the storm are due to the spread of heat in the auroral oval neutral wind to mid-latitudes. The fact that, in winter conditions, the negative response propagates with a delay and does not reach low latitudes allows for an attempt to determine the speed of its propagation from high to mid-latitudes. An approximate value of about 650 m/s was obtained, confirming the hypothesis of Fuller-Rowell [4] for the excitation of a gravity wave with a phase velocity of this order.

In general, the variations in the peak height of the F2-layer have an opposite character to the variations in critical frequencies and TEC. They are strongest at night and vary in geomagnetic storm conditions, which this study confirms [39].

In this present paper, the positive pre-storm anomaly in the critical frequencies measured in Europe is examined in detail. The peculiar manifestation of this anomaly is due to the fact that such an effect is absent in the TEC data, which means that the increase in the maximum electron density is compensated by a decrease in the region above the maximum. The atypical reaction of the ionosphere gives us a reason to consider this anomaly a product of intra-atmospheric processes.

Author Contributions: Conceptualization, P.M. and R.B.; methodology, P.M.; software, P.M. and R.B.; validation, P.M.; formal analysis, R.B.; investigation, P.M. and R.B.; resources, P.M.; data curation, P.M. and R.B.; writing—original draft preparation, R.B.; writing—review and editing, R.B.; visualization, R.B.; supervision, R.B. All authors have read and agreed to the published version of the manuscript.

Funding: This work has been carried out in the framework of the National Science Program "Environmental Protection and Reduction of Risks of Adverse Events and Natural Disasters" approved by the Resolution of the Council of Ministers № 577/17.08.2018 and supported by the Ministry of Education and Science (MES) of Bulgaria (Agreement № 01-271/09.12.2022). This work was partially supported by the Bulgarian Ministry of Education and Science under the National Research Programme "Young scientists and postdoctoral students-2", approved by DCM № 206 /07.04.2022.

Data Availability Statement: The TEC data provided by CODE are available at: ftp://ftp.unibe.ch/aiub/CODE/, accessed on 25 July 2023. The data for the parameters hmF2 and foF2 from selected ionospheric stations provided by the GLOBAL IONOSPHERE RADIO OBSERVATORY (GIRO) can be found at the following address: https://giro.uml.edu/didbase/scaled.php, accessed on 25 July 2023. The parameters Bz component of IMF and density of solar wind are provided by NASA Advanced Composition Explorer (ACE) satellite ftp://ftp.swpc.noaa.gov/pub/lists/ace/, accessed on 25 July 2023. All of the indices Dst index, Kp index, and F10.7 are taken from https://omniweb.gsfc.nasa.gov/, accessed on 20 July 2023. The Power index (available at this address http://services.swpc.noaa.gov/text/aurora-nowcast-hemi-power.txt, accessed on 24 July 2023) and data about stratospheric temperature and solar wind speed (https://www.cpc.ncep.noaa.gov/products/monitoring_and_data/oadata.shtml, accessed on 21 July 2023) were obtained from NATIONAL OCEANIC AND ATMOSPHERIC ADMINISTRATION (NOAA), Space Weather Prediction Center.

Acknowledgments: We are grateful to CODE for the access to the TEC data and to Goddard Space Flight Center for the freely available data of the Bz component, Dst index, and Kp index. The authors express special thanks to the ionospheric data kindly provided by the Global Ionosphere Radio Observatory. The authors express their gratitude to NOAA-Space Weather Prediction Center.

Conflicts of Interest: The authors declare no conflict of interest.

References

1. Rishbeth, H. F-region storms and thermospheric dynamics. *J. Geomagn. Geoelectr.* **1991**, *43*, 513–524. [CrossRef]
2. Werner, S.; Bauske, R.; Prolss, G.W. On the origin of positive ionospheric storms. *Adv. Space. Res.* **1999**, *24*, 1485–1489. [CrossRef]
3. Mikhailov, A.; Schlegel, K. Physical mechanism of strong negative storm effects in the daytime ionospheric F2 region observed with EISCAT. *Ann. Geophys.* **1998**, *16*, 602–608. [CrossRef]
4. Fuller-Rowell, T.J.; Codrescu, M.V.; Moffett, R.J.; Quegan, S. Response of the thermosphere and ionosphere to geomagnetic storms. *J. Geophys. Res. Space Phys.* **1994**, *99*, 3893–3914. [CrossRef]
5. Danilov, A.D.; Lastovicka, J. Effects of geomagnetic storms on the ionosphere and atmosphere. *Int. J. Geomagn. Aeron.* **2001**, *2*, 209–224.

6. Rishbeth, H. How the thermospheric circulation affects the ionospheric F2-layer. *J. Atmos. Sol.-Terr. Phys.* **1998**, *60*, 1385–1402. [CrossRef]
7. Astafyeva, E.; Bagiya, M.S.; Förster, M.; Nishitani, N. Unprecedented hemispheric asymmetries during a surprise ionospheric storm: A game of drivers. *J. Geophys. Res. Space Phys.* **2020**, *125*, e2019JA027261. [CrossRef]
8. Wang, Z.; Zou, S.; Liu, L.; Ren, J.; Aa, E. Hemispheric Asymmetries in the Mid-latitude Ionosphere During the September 7–8, 2017 Storm: Multi-instrument Observations. *J. Geophys. Res. Space Phys.* **2021**, *126*, e2020JA028829. [CrossRef]
9. Zhai, C.; Cai, X.; Wang, W.; Coster, A.; Qian, L.; Solomon, S.; Yu, T.; He, M. Mid-Latitude Ionospheric Response to a Weak Geomagnetic Activity Event During Solar Minimum. *J. Geophys. Res. Space Phys.* **2023**, *128*, e2022JA030908. [CrossRef]
10. Balan, N.; Liu, L.; Le, H. A brief review of equatorial ionization anomaly and ionospheric irregularities. *Earth Planet. Phys.* **2018**, *2*, 257–275. [CrossRef]
11. Karan, D.K.; Eastes, R.W.; Daniell, R.E.; Martinis, C.R.; McClintock, W.E. GOLD mission's observation about the geomagnetic storm effects on the nighttime equatorial ionization anomaly (EIA) and equatorial plasma bubbles (EPB) during a solar minimum equinox. *Space Weather* **2023**, *21*, e2022SW003321. [CrossRef]
12. Wu, K.; Qian, L.; Wang, W.; Cai, X.; Mclnerney, J.M. Investigation of the GOLD observed merged nighttime EIA with WACCM-X simulations during the storm of 3 and 4 November 2021. *Geophys. Res. Lett.* **2023**, *50*, e2023GL103603. [CrossRef]
13. Astafyeva, E.; Yasyukevich, Y.V.; Maletckii, B.; Oinats, A.; Vesnin, A.; Yasyukevich, A.S.; Syrovatskii, S.; Guendouz, N. Ionospheric disturbances and irregularities during the 25–26 August 2018 geomagnetic storm. *J. Geophys. Res. Space Phys.* **2022**, *127*, e2021JA029843. [CrossRef]
14. Bojilova, R.; Mukhtarov, P. Comparative Analysis of Global and Regional Ionospheric Responses during Two Geomagnetic Storms on 3 and 4 February 2022. *Remote Sens.* **2023**, *15*, 1739. [CrossRef]
15. Goncharenko, L.P.; Coster, A.J.; Chau, J.L.; Valladares, C.E. Impact of sudden stratospheric warmings on equatorial ionization anomaly. *J. Geophys. Res. Space Phys.* **2010**, *115*, A00G07. [CrossRef]
16. O'Neill, A. Stratospheric sudden warmings. In *Encyclopedia of Atmospheric Sciences*; Holton, J.R., Pyle, J.A., Curry, J.A., Eds.; Elsevier: New York, NY, USA, 2003; pp. 1342–1353.
17. Goncharenko, L.; Zhang, S.R. Ionospheric signatures of sudden stratospheric warming: Ion temperature at middle latitude. *Geophys. Res. Lett.* **2008**, *35*, L21103. [CrossRef]
18. Pancheva, D.; Mukhtarov, P. Stratospheric warmings: The atmosphere–ionosphere coupling paradigm. *J. Atmos. Sol.-Terr. Phys.* **2011**, *73*, 1697–1702. [CrossRef]
19. Lin, J.T.; Lin, C.H.; Chang, L.C.; Huang, H.H.; Liu, J.Y.; Chen, A.B.; Chen, C.H.; Liu, C.H. Observational evidence of ionospheric migrating tide modification during the 2009 stratospheric sudden warming. *Geophys. Res. Lett.* **2012**, *39*, L02101. [CrossRef]
20. Oyama, K.I.; Jhou, J.T.; Lin, J.T.; Lin, C.; Liu, H.; Yumoto, K. Ionospheric response to 2009 sudden stratospheric warming in the Northern Hemisphere. *J. Geophys. Res. Space Phys.* **2014**, *119*, 10260–10275. [CrossRef]
21. Mukhtarov, P.; Pancheva, D. Winter-time dependence of the global TEC on the stratospheric temperature and solar radiation. *J. Atmos. Sol.-Terr. Phys.* **2015**, *136*, 134–149. [CrossRef]
22. Pedatella, N.M. Impact of the lower atmosphere on the ionosphere response to a geomagnetic superstorm. *Geophys. Res. Lett.* **2016**, *43*, 9383–9389. [CrossRef]
23. Vijaya, G.; Arumugam, S. Monitoring the stability of the processes in defined level software companies using control charts with three sigma limits. *WSEAS Trans. Inf. Sci. Appl.* **2010**, *7*, 1230–1239.
24. Ciraolo, L.; Azpilicueta, F.; Brunini, C.; Meza, A.; Radicella, S.M. Calibration errors on experimental slant total electron content (TEC) determined with GPS. *J. Geod.* **2007**, *81*, 111–120. [CrossRef]
25. Schaer, S. Mapping and Predicting the Earths Ionosphere Using the Global Positioning System. Ph.D. Thesis, University of Bern, Bern, Switzerland, 1999; p. 205.
26. Chau, J.L.; Goncharenko, L.P.; Fejer, B.G.; Liu, H.L. Equatorial and low latitude ionospheric effects during sudden stratospheric warming events: Ionospheric effects during SSW events. *Space Sci. Rev.* **2012**, *168*, 385–417. [CrossRef]
27. Goncharenko, L.; Chau, J.L.; Condor, P.; Coster, A.; Benkevitch, L. Ionospheric effects of sudden stratospheric warming during moderate-to-high solar activity: Case study of January 2013. *Geophys. Res. Lett.* **2013**, *40*, 4982–4986. [CrossRef]
28. Fang, T.W.; Fuller-Rowell, T.; Akmaev, R.; Wu, F.; Wang, H.; Anderson, D. Longitudinal variation of ionospheric vertical drifts during the 2009 sudden stratospheric warming. *J. Geophys. Res. Space Phys.* **2012**, *117*, A03324. [CrossRef]
29. Jonah, O.F.; De Paula, E.R.; Kherani, E.A.; Dutra, S.L.; Paes, R.R. Atmospheric and ionospheric response to sudden stratospheric warming of January 2013. *J. Geophys. Res. Space Phys.* **2014**, *119*, 4973–4980. [CrossRef]
30. Sumod, S.G.; Pant, T.K.; Jose, L.; Hossain, M.M.; Kumar, K.K. Signatures of sudden stratospheric warming on the equatorial ionosphere-thermosphere system. *Planet. Space Sci.* **2012**, *63*, 49–55. [CrossRef]
31. Butler, A.H.; Seidel, D.J.; Hardiman, S.C.; Butchart, N.; Birner, T.; Match, A. Defining sudden stratospheric warmings. *Bull. Am. Meteorol. Soc.* **2015**, *96*, 1913–1928. [CrossRef]
32. Adebesin, B.O.; Ikubanni, S.O.; Kayode, J.S.; Adekoya, B.J. Variability of solar wind dynamic pressure with solar wind parameters during intense and severe storms. *Afr. Rev. Phys.* **2013**, *8*, 119–128.
33. Laštovička, J. Effects of geomagnetic storms in the lower ionosphere, middle atmosphere and troposphere. *J. Atmos. Sol.-Terr. Phys.* **1996**, *58*, 831–843. [CrossRef]

34. Blagoveshchenskii, D.V. Effect of geomagnetic storms (substorms) on the ionosphere: 1. A review. *Geomagn. Aeron.* **2013**, *53*, 275–290. [CrossRef]
35. Buresova, D. Effects of geomagnetic storms on the bottomside ionospheric F region. *Adv. Space. Res.* **2005**, *35*, 429–439. [CrossRef]
36. Immel, T.J.; Mannucci, A.J. Ionospheric redistribution during geomagnetic storms. *J. Geophys. Res. Space Phys.* **2013**, *118*, 7928–7939. [CrossRef] [PubMed]
37. Nava, B.; Rodríguez-Zuluaga, J.; Alazo-Cuartas, K.; Kashcheyev, A.; Migoya-Orué, Y.; Radicella, S.M.; Amory-Mazaudier, C.; Fleury, R. Middle-and low-latitude ionosphere response to 2015 St. Patrick's Day geomagnetic storm. *J. Geophys. Res. Space Phys.* **2016**, *121*, 3421–3438. [CrossRef]
38. Andonov, B.; Muhtarov, P.; Kutiev, I. Analogue model, relating Kp index to solar wind parameters. *J. Atmos. Sol.-Terr. Phys.* **2004**, *66*, 927–932. [CrossRef]
39. Bojilova, R.; Mukhtarov, P. Response of the electron density profiles to geomagnetic disturbances in January 2005. *Stud. Geophys. Geod.* **2019**, *63*, 436–454. [CrossRef]
40. Danilov, A.D. Prestorm ionospheric disturbances: Precursors or Q-disturbances? *Adv. Space Res.* **2022**, *69*, 159–167. [CrossRef]
41. Danilov, A.D.; Konstantinova, A.V. Ionospheric precursors of geomagnetic storms. 1. A review of the problem. *Geomagn. Aeron.* **2019**, *59*, 554–566. [CrossRef]
42. Burešová, D.; Laštovička, J. Pre-storm enhancements of foF2 above Europe. *Adv. Space Res.* **2007**, *39*, 1298–1303. [CrossRef]
43. Mikhailov, A.V.; Perrone, L. Pre-storm NmF2 enhancements at middle latitudes: Delusion or reality? *Ann. Geophys.* **2009**, *27*, 1321–1330. [CrossRef]
44. Andonov, B.; Bojilova, R.; Mukhtarov, P. Global distribution of total electron content response to weak geomagnetic activity. *CR Acad. Bulg. Sci.* **2021**, *74*, 1032–1042.
45. Okoh, D.; Bounhir, A.; Habarulema, J.B.; Rabiu, B.; Katamzi-Joseph, Z.; Ojo, T.; Wu, Q.; Makela, J.J. Thermospheric Neutral Wind Measurements and Investigations across the African Region—A Review. *Atmosphere* **2022**, *13*, 863. [CrossRef]